Bi-linearity in the Gutenberg-Richter relation based on M_L for magnitudes above and below 2, from systematic magnitude assessments in Parkfield (California)

Nadine Staudenmaier*[1], Thessa Tormann[1], Benjamin Edwards[2], Nicholas Deichmann[1] and Stefan Wiemer[1]

[1] Swiss Seismological Service, ETH Zurich, Zurich, Switzerland.

[2] Department of Earth, Ocean and Ecological Sciences, University of Liverpool, Liverpool, UK.

Corresponding author: Nadine Staudenmaier (nadine.staudenmaier@sed.ethz.ch)

Key Points:

- Scaling break between local magnitude and moment magnitude
- Different slopes of the earthquake frequency-magnitude distribution for local magnitudes below and above 2.0
- Seismic hazard studies need to carefully consider these scaling breaks.

Revised manuscript submitted to GRL on 24th May 2018

Abstract

Several studies have shown that local magnitude, M_L, and moment magnitude, M, scale differently for small earthquakes (M<~2) than for moderate to large earthquakes. Consequently, frequency-magnitude relations based on one or the other magnitude type cannot obey a power-law with a single exponent over the entire magnitude range. Since this has serious consequences for seismic hazard assessments, it is important to establish for which magnitude type the assumption of a constant exponent is valid and for which it is not. Based on independently determined M, M_L and duration-magnitude, M_d, estimates for 5304 events near Parkfield, we confirm the theoretically expected difference in scaling between the magnitude types, and we show that the frequency-magnitude distribution based on M and M_d follows a Gutenberg-Richter relation with a constant slope, whereas for M_L it is bi-linear. Thus, seismic hazard estimates based on M_L of small earthquakes are likely to overestimate the occurrence probability of large earthquakes.

1 Introduction

A central and seemingly straightforward task in seismology is the precise estimation of earthquake size. This forms a pre-requisite to characterize and compare events and to study their relative frequency of occurrence. Unfortunately, estimating the size of an earthquake is non-trivial. Numerous magnitude scales have been developed and are used in various implementations to produce earthquake catalogs (i.e. local-, moment-, energy-, duration-, body-, or surface wave magnitudes), and each of these magnitude types describes different characteristics of an event. The oldest and most well-known instrumental magnitude scale is the Richter magnitude, or local magnitude, M_L (Richter, 1935). It is determined from the peak-amplitude of the horizontal ground displacement recorded by a Wood-Anderson seismograph. However, local magnitude needs careful attenuation calibration and suffers strongly from saturation effects for larger earthquakes (Aki and Richards, 2002). The duration magnitude, M_d, reflects the length of the waveform signal, from the onset of the P-wave until the coda amplitude falls below a certain level (Eaton, 1997). For seismic hazard analyses, moment magnitude (**M**) is the preferred choice of magnitude. **M** is based on the seismic moment (M_0), which is proportional to the product of fault area and average slip of the rupture (with constant rigidity). Similarly to the seismic moment, **M** is a purely static measure of earthquake size and, consequently, can also be estimated for paleo-earthquakes (e.g., Fäh et al., 2011). Moment magnitude has furthermore the advantage not to be affected by saturation effects that influence most other scales. The seismic moment and thus **M** are commonly estimated from the low-frequency plateau of the Fourier amplitude spectra of the recorded displacement waveforms, which for small earthquakes is technically challenging and limited by ambient noise levels (Edwards et al., 2010; Stork et al., 2014). To include as many earthquakes as possible in their catalogs, to facilitate automated and rapid processing and for consistency, monitoring network operators therefore still prefer magnitude estimates based on simply measurable parameters such as signal duration (M_d) or peak-amplitudes (M_L). Consequently, for seismic hazard analyses, the amplitude based magnitude estimates reported in the catalogs (typically M_L) are, in contemporary hazard studies, subsequently converted to moment magnitudes via empirically derived regression formulas (e.g. Goertz-Allmann et al., 2011).

The frequency-magnitude-distribution (FMD) of earthquakes is usually well described by a power law, expressed often as the truncated Gutenberg-Richter relation (Gutenberg and Richter, 1944):

$$\log(N)=a-bM \qquad M \leq M_{max} \tag{1}$$

where N is the number of events equal to or greater than magnitude M, a (activity rate) and b (size distribution) are constants and M_{max} is the maximum considered magnitude. This relationship is commonly used to characterize fault zones and to derive the expected recurrence rates of rare large events by extrapolating from the observed activity rate (a-value) and size distribution (b-value) of abundant small to moderate seismicity (Aki, 1987; Abercrombie and Brune, 1994; Wiemer et al., 2009). Thus, the quality of seismic hazard assessment, but also of many other studies in statistical seismology or earthquake source physics, strongly depends on the *consistency* of magnitude assessments with respect to time, space and magnitude.

Intuitively, the expectation appears reasonable that an earthquake has a single ‘magnitude’ and each measure (M_d, M_L, **M**,…) should result in the same broadly consistent value for properly calibrated scales, with some scatter. However, this is not the case: independent estimates of different earthquake properties can lead to systematic and significant differences between the scales, particularly for extrapolations outside of the initial calibration range. A particularly important and often reported scaling break between magnitude scales has been observed at small magnitudes ($M < 3$) between local magnitude (M_L) and moment magnitude ($\mathbf{M}$) Given M_L=c$\mathbf{M}$+d, it has been observed that for M_L between 3 and 6 the proportionality coefficient c is close to 1 (Bakun, 1984; Hanks and Boore, 1984). However, below $\mathbf{M}$=3, c increases and has been reported to be around 1.3 to 1.6 (Bakun, 1984; Hanks and Boore, 1984; Goertz-Allmann et al., 2011; Edwards and Douglas, 2014; Ross et al., 2016, Bethmann et al., 2011, Munafò et al., 2016, Deichmann 2017). This break in scaling between the two magnitude scales implies that constant power-law scaling must break down for at least one of the two scales. Despite considerable efforts, until today it is not empirically demonstrated which of the two scales leads to deviation from the simple power-law FMD (Equation 1), and this lack of understanding has had major implication for site specific as well as national seismic hazard and various tectonic stress and b-value studies (e.g., Wiemer et al., 2015;Wiemer and Wyss, 2002; Tormann et al., 2012 and 2014).

Recent theoretical and empirical studies predict a ratio of 1.5:1 between M_L and $\mathbf{M}$ (c=1.5) for small earthquakes, due to surface attenuation imposing a minimum limit to the observed pulse duration (Edwards et al., 2015, Deichmann, 2017). The same conclusion can be drawn based on random vibration theory, noting that, given the upper cut-off frequency of the attenuating media, peak displacement amplitudes are logarithmically proportional to the seismic moment for earthquakes with corner frequencies above the upper limit of this pass-band (e.g. Munafò et al., 2016).

To address this question, we conduct a magnitude scaling assessment on data over a wide magnitude range, based on independently calculated magnitude estimates. We process local earthquake data in the data-rich and well monitored Parkfield region in California, and estimate the most common magnitude types, $\mathbf{M}$, M_L and M_d. To obtain a consistent data set, we use a single borehole station. The earthquakes in the study region span a wide magnitude range, from well below to well above the suggested break point in the scaling relationship between M_L and $\mathbf{M}$. We explore the relations between the different scales and discuss the implications and potential pitfalls for hazard assessment and other earthquake studies.

2 Setting and Network

The Parkfield segment of the San Andreas Fault (SAF) is one of the best-monitored and most extensively studied fault segments in the world (Bakun and Lindh, 1985). It has long been recognized as an ideal natural laboratory for studying crustal fault phenomena (i.e. Bakun, 2005). The Parkfield segment has ruptured repeatedly with **M**6 events on average every 20-25 years (6 times since 1857). Dense networks of various geophysical instruments have been installed at the site of the 'Parkfield Experiment' and a tremendous amount of data of high quality have been collected with the intention to reveal potential precursors to **M**6 events (HRSN, 2014). The most recent **M**6 event occurred in 2004 after the longest observed inter-event time of about 38 years.

To monitor microseismicity accompanying the larger events, the High Resolution Seismic Network (HRSN) was installed (HRSN, 2014). It is operated by the Berkeley Seismological Laboratory and is a 13-station array of geophone borehole instruments (each 3 channels) with a sampling rate of 250Hz. The stations are located on both sides of the fault (Figure 1) at 63 to 345 m depth (HRSN, 2014). While the noise level for borehole stations is generally much lower than for a surface network, there are still significant differences between the 13 stations. Upgrades of the instruments have been performed at different times over the last decade to improve signal-to-noise ratios.

Due to site effects, ambient noise levels, and instrument upgrades happening at different times, the signal-to-noise ratio of the earthquake recordings varies significantly between stations. Magnitudes determined as an average of several recordings may therefore introduce systematic bias, depending on the stations used for each event. We therefore restrict our dataset to the recordings of a single reference station: SMNB (Stockdale Mountain Borehole). The station is the third deepest in the HRSN, with the sensor depth of 282 m below the surface, and was selected due to very low noise and undisturbed recording over long periods (Staudenmaier et al., 2016).

3 Earthquake data

Within the study region, we used the Northern California Earthquake Data Center (NCSN) catalog events from mid-2001 to the end of 2016, excluding the **M**6 event (catalog magnitude of 5.97) in September 2004 due to clipped signals at the reference station. We restricted our choice of events to seismicity along the SAF, including the Parkfield asperity and part of the creeping segment to the north (Figure 1).

To investigate the fundamental scaling properties between magnitudes, it is ideal to analyze the relative magnitudes of events with similar hypocentral locations and similar focal mechanisms recorded by a single station. Along this part of the SAF, the focal mechanisms of most of the events close to the fault are purely strike-slip. To include a sufficiently large number of events for a statistically significant frequency-magnitude distribution, it was necessary to use data from an extended fault-segment, rather than events originating from a very restricted hypocenteral area (Figure 1).

The catalog data shows an increase in seismicity rate after the **M**6 event. However, our detailed analysis of the NCSN catalogue revealed that during ~18 months following the 2004 **M**6 event, an average of 30% (and up to 80%, e.g. 21 Nov 2004) of the events in the catalogue have unknown magnitude. For 5631 events with given catalog magnitudes, we retrieved the recorded waveform signal at the reference station, with a window of 5s before and 25s after the event. This extension before and after the event signal reduced the data set to 5344 events due to excluding the time-overlapping waveforms, mostly detected in the aftershock series of the **M**6 event of 2004.

4 Magnitude determination

Based on the retrieved waveform data, we independently determine M_L, M_d and **M**, i.e. we do not apply any conversion from one magnitude to another. For the analysis we used all three components of the station.

4.1 Local magnitude M_L

The main motivation to introduce local magnitude has been to provide a simple quantitative measure of the relative size distribution of earthquakes (Richter, 1935). It is based on the displacement in mm on a Wood-Anderson (WA) Torsion Seismometer (A)

$$M_L = log_{10}A + f\left(R_{hyp}\right), \quad (2)$$

along with the distance correction $f(R_{hyp})$ modified from Kanamori et al., (1993) for the source-receiver (hypocentral) distance R_{hyp} (in km):

$$f(R) = -\log(0.3173\exp(-0.00505R_{hyp})\,{R_{hyp}}^{-1.14}) \quad (3)$$

With Parkfield being located very close to the Northern and Southern California boundary we used the SCSN formulation for distance correction *f(R_{hyp}):* The justification for this is that the SCSN calculates M_L estimates for all events, while the NCSN uses M_L estimates only for events above magnitude 3.

4.2 Duration magnitude M_d

Observing that WA seismometers, because of low magnification, did not provide useful records for events smaller than magnitude 2, Lee et al. (1972) introduced a signal-duration based magnitude for the NCSN:

$$M_d = -0.87 + 2.00 \log(\tau) + 0.0014 R_{epi}\ ,\ 0.5 < M < 5, \tag{3}$$

where τ represents the signal duration in seconds and R_{epi} is the epicentral distance in kilometres.

Originally, the event duration was measured from the onset of the P-wave to the point on the seismogram where the coda amplitude diminished to 1 cm amplitude (post gain) on the Develocorder film viewer screen. The signal duration definition varies from study to study (Lee et al., 1972, Eaton, 1992). Based on our results, we defined the signal duration on the 5-95% cumulative squared velocity integral of the signal. To test for stability and consistency of this choice, we also calculated duration magnitude estimates for signal duration defined by 2-98% and 10-90%. While different definitions of duration lead to significant changes of absolute magnitude estimates, the relative magnitude distribution is unaffected.

4.3 Moment magnitude M

According to Hanks and Kanamori (1979) moment magnitude, **M**, is related to seismic moment M_0 (in Nm) by

$$\mathbf{M} = \frac{2}{3}(\log_{10} \mathrm{M}_0 - 9.05) \tag{5}$$

The seismic moment is calculated as:

$$M_0 = \frac{4\pi\beta_0^3\rho_0}{FS} U_0 G(R) \quad (6)$$

where F is the average radiation coefficient (0.55 for SH waves), β is the near-source shear-wave velocity (3500 m/s), S is the free-surface amplification (2.0 for SH waves), ρ is the average crustal density (2700 kg m^{-3}), U_0 is the low-frequency level (plateau) of the displacement spectrum and G(R) is the geometrical spreading function (Aki and Richards, 2002; Atkinson and Silva, 1997). To determine the plateau of the displacement spectrum, we apply a spectral fitting method as documented in Edwards et al. (2010) using a maximum frequency band of 1 to 125 Hz. The Fourier spectrum is then limited to the range where the signal to noise ratio exceeds three. We use the Californian Q and corresponding geometrical spreading model of Raoof et al (1999) to account for path attenuation along with a site specific κ0 of 0.01s.

5 Results

Following the procedures as outlined above, we obtained moment-, local-, and duration magnitude estimates for 5304 events for which signal quality was sufficient (signal-to-noise ratio > 3). In this section, we compare the scaling relations of these different magnitudes. We use a weighted total least-squares algorithm that minimizes errors of both variables to compute the regressions for the coefficient of proportionality c between two magnitude scales (Krystek and Anton, 2007). Defining an uncertainty estimate for our obtained magnitudes is not as straightforward as for magnitudes derived at several stations. We tested the sensitivity to parameters that may affect the magnitude estimate, such as: the length of time windows for detection, different signal-to-noise used in the spectral analysis, and the influence of distance and lateral location uncertainty as well as the impact of radiation pattern, path and site effects. Each of this parameter can contribute up to ± 0.1-0.3 units of magnitude for each variable (Bethmann et al., 2011;Stork et al., 2014), which is about 6-10 % in the magnitude range of interest. The resulting error on magnitude is between 0.1 and 0.3 magnitude units, depending on magnitude type and event. We therefore assume an average error estimate of 0.2 for all magnitude scales.

5.1 Comparison of duration magnitude: Md vs. ($M_{d,NCSN}$)

To evaluate whether the obtained duration magnitudes are reliable, we compared them with the NCSN catalog estimates, which contains only duration magnitudes for events smaller than 3. We found that the independently calculated magnitudes from the present study are in good agreement with the catalog values: The regression over the available data ($M_{d,NCSN}$ between 0 and 3) yields M_d=(1.042±0.031)$M_{d,NCSN}$+0.15. The standard deviation of the data with respect to the regression amounts to 0.17 (supporting information figure S1). This means, the independently calculated magnitudes from the single borehole station are, on average, 0.15 lower than the catalog estimates derived as an average over several stations. This shift can be explained by site-amplification of the station (where we would typically expect shorter durations at the borehole level) or by the different evaluation of the signal duration. Since we are interested in relative scaling between different magnitude types, the absolute shift is, nevertheless, unimportant in the scope of this work.

5.2 Duration and moment magnitude (M_d vs. M)

We now compare our moment magnitudes estimates obtained from spectral analysis and the magnitude determined form signal durations. Both magnitude estimates give similar values: over the whole range of analysis (**M** -1 to 4.7), the regression results in M_d=(1.061±0.02)**M** + 0.11 (supporting information figure S2). The overall standard deviation of the data with respect to the regression is 0.37.

5.3 Local magnitudes (M_L) versus moment magnitudes (M)

The comparison of moment magnitudes obtained from spectral analysis and local magnitudes determined from signal amplitude shows that a single linear regression over the entire magnitude range does not do justice to the data. Even in a plot of M_L versus **M** (upper inset in Figure 3) one sees that the coefficient of proportionality is greater for smaller events than for larger events. This is even more evident in a plot of (M_L - **M**) versus M_L in Figure 2b, which is similar to a corresponding plot for Swiss data (Goertz-Allmann et al., 2011), shown here in Figure 2a. If we fit the data of M_L versus **M** separately for **M** < 2.2 and **M** > 2.5, we obtain a coefficient of proportionality of 1.46 ± 0.022 for the smaller events and of 1.04 ± 0.030 for the larger ones. We thus observe a break in the scaling of M_L and **M** between smaller and larger earthquakes. To test the stability of the scaling relation for events smaller than **M** 2, we applied bootstrapping to the catalog. This results in a stable scaling factor between M_L and **M** of 1.47 +/- 0.034 for **M** < 2.

5.4 Break in scaling between M and M_L

The key to understanding the reason for the break in scaling between M_L and **M** is the fact that as the magnitudes decrease, the corner frequencies of the spectra observed at a particular site approach a finite maximum. This means that observed corner frequencies or equivalently the observed pulse widths remain nearly constant independently of the event magnitude. In this case, log(A) and thus M_L scale 1:1 with log(M_0), which in turn is equivalent to a scaling of 1.5:1 of M_L versus **M** (e.g. Edwards et al., 2015; Munafò et al., 2016; Deichmann, 2017). Harrington and Brodsky (2009) already observed that, for earthquakes on the San Andreas fault near Parkfield, pulse widths remain nearly constant over a large magnitude range, although they interpreted this as evidence for a minimum source size, rather than a site attenuation effect.

The lower inset in Figure 3 shows the normalized velocity spectra resulting from the spectral fitting procedure of Edwards et al. (2010), used in this study for the estimate of **M**. Each spectrum is the best-fitting product of the velocity spectrum of a Brune source model and the modified frequency response of the attenuation model for Southern California of Raoof et al. (1999). The modification of the attenuation model concerns κ, the contribution of the receiver site, which was decreased to 0.01 s, to account for our use of borehole recordings. We note that uncertainty is associated with the parameters obtained in this fitting procedure: however, in our case we are interested in visualizing the spectral shape only (which by definition is minimized with respect to the data). The maximum corner frequency fitted to the empirical data is around 30 Hz. This value corresponds closely to the corner frequency of the frequency response of the modified attenuation model of Raoof et al. (1999) computed for a hypocentral distance of 1 km (31.3 Hz). In other words, the attenuation model of Raoof et al. (1999) is sufficient to account for the observed upper corner-frequency limit. Contrary to Harrington and Brodsky (1999) and from the coincidence between the observed maximum corner frequency and the corner frequency of the ground motion model, conclude that the break in scaling is not a source effect but a consequence of an-elastic attenuation and scattering between source and receiver.

5.5 Consequences for Gutenberg-Richter power-law scaling and probabilistic seismic hazard analysis

Given the observed difference in scaling of M_L versus **M** for small and large events, it is obvious that recurrence rates derived from the slope (b-value) of a frequency-magnitude distribution (FMD) must also be different for small and large earthquakes. In particular, as shown in Figures 3b and 3c, if the FMD is linear for **M** over the entire magnitude range, it cannot be linear for $M_{L,}$ and vice-versa. The FMD's with respect to our three independently determined magnitudes plotted in Figure 3 show clearly that for M_L, contrary to M_d and **M**, the FMD is characterized by a pronounced bend between about M_L 1.5 and 2.5 and thus cannot be fitted by a single straight line over the entire magnitude range. For magnitudes above about 2.1, the b-value for M_L is 0.85 and, within the uncertainty of +/-0.03 estimated according to Shi and Bolt (1982), is essentially identical to the b-values for M_d (0.87) and **M** (0.88), determined over the entire range of completeness (M_c = 1.21 and 1.02). However, with b = 0.51, the slope of the FMD determined for events with M_L less than about 1.9 is significantly lower. We also found this observation to be stable for different time periods.

6 Discussion and conclusions

One-to-one scaling between the **M** and M_L scales breaks down between magnitudes 2 and 3. This fact has been empirically established for many regions (Bakun, 1984; Hanks and Boore, 1984; Goertz-Allmann et al., 2011; Edwards and Douglas, 2014; Bethmann et al., 2011; Ross et al., 2016; Munafò et al., 2016). Our results show while the b-value inferred from **M** remains approximately constant across the magnitude range, that the estimate from ML is lower at lower magnitudes.

Our work (Figure 2, 3) confirms this finding with a highly consistent dataset and thus highlights once more the intrinsic dangers of converting from M_L to **M**, or vice-versa. The proposal that surface attenuation imposes a minimum limit to the observed pulse duration, or equivalently a maximum limit to the corner frequency of the observed spectra (e.g. Edwards et al., 2015, Deichmann, 2017) is consistent with our findings. It is likely that the exact shape of the M_L to **M** relationship is regionally variable, depending on network characteristics, source properties, attenuation and local site effects. Although the focal mechanisms of the events in our data set are all very similar to each other, differences in take-off angles due to different hypocenter locations introduce a dependence of **M** and M_L on the radiation pattern.

Adopting an average radiation coefficient to compute M_0 from Equation 6 just adds a constant vertical shift to the curve in Figure 2b, and with regard to the slope of the curve it is equivalent to ignoring possible contributions of the radiation pattern. In a homogeneous medium this would be justified, since the radiation pattern is identical for both the low-frequency level of the displacement spectrum and the maximum amplitude of the ground displacement. For frequencies below about 2 Hz, this can also be expected in the case of a heterogeneous medium (Takemura et al., 2009). At higher frequencies, however, scattering due to small-scale heterogeneities along the wavepath has a smoothing effect on the azimuthal dependence of the wavefield. With increasing hypocentral distance, this smoothing effect can lead to a nearly isotropic apparent radiation pattern of the SH-waves (Takemura et al., 2009). In this case, our estimate of M_0 based on frequencies below 2 Hz would show the source-specific dependence on the radiation pattern, whereas our estimate of M_L, based on the maximum displacement amplitude, that is, in most cases, measured at substantially higher frequencies, would show a significantly weaker azimuthal dependence. Consequently, ignoring the event-specific radiation pattern in our computations of M_0 introduces a potential discrepancy between our estimates of **M** and M_L and thus contributes to the vertical scatter of the data points in Figure 2b.

In our case, the scaling of M_L to **M** from recordings of events with mostly similar focal mechanisms and distributed over a limited region observed at a single station is practically identical to the theoretically expected 1.5:1 scaling for small events. However, in earthquake catalogs of events with different focal mechanisms recorded over different distances and with magnitudes based on averages from multiple stations, the scaling coefficient for small magnitudes can deviate from the expected value of 1.5 (e.g. 1.33 in Ross et al., 2016, or 1.68 in Goertz-Allmann et al. 2011). Given the large number of parameters that are involved, the explanation for these observed discrepancies is not straightforward.

It is worthwhile noting that duration magnitude, M_d, scales very well with **M**, suggesting that duration can be a suitable proxy for **M** (e.g. Edwards and Douglas, 2014). One open question is the absolute calibration of M_d, with differences in definition of duration leading to systematic shifts between different measures of M_d. This may be regionally variable, as near-surface deposits are known to strongly influence the duration of shaking. We therefore caution the interpretation of activity rates (*a*-value) inferred from M_d to **M** conversions, but presume that given M_d to **M** pairs (from independent measurement) this could be empirically calibrated.

Our findings confirm the theoretical considerations of M_L scaling breaks by Edwards (2015) and Deichmann (2017). In principle, our study resolves the scaling related issues that have plagued many hazard and statistical seismology related studies in the past decade. For analyses of b-values or extrapolations of recurrence rates, earthquake catalogs reported in M_L cannot be reliably used below magnitudes of around 2.5 without region-specific non-linear adjustments. This has a significant effect on seismic hazard assessment, as only the slope (b-value) for M>2.5 can be extrapolated with confidence to estimate recurrence rates for higher magnitudes. This is especially challenging for settings that lack sufficient M>2.5 events but that do record abundant smaller events, e.g. induced seismicity, in which densely spaced networks are located very close to the events. Those events are often processed using the M_L approach, and, based on the results presented in this study, we argue that it is indispensable to calculate moment magnitudes from the displacement spectrum, at least for a data subset. From this it is then possible to determine the appropriate scaling at the study site and accordingly correct the M_L values for those events for which **M** is not available. Only then, is an extrapolation of the size distribution for seismic hazard assessment possible.

The results of our magnitude analysis, which is based on a relatively homogenous data set recorded at a single station, clearly show that the bend in the FMD occurs for M_L and not for **M**. In FMD plots based on regional earthquake catalogs, that are much more heterogeneous (e.g. Switzerland, Southern California, Japan), this is not so clear. In these cases, the FMDs based on M_L can actually be approximated by a single straight line over the whole magnitude range. Whether this is an artifact of the usual distance calibration of M_L, which might inadvertently compensate for the underestimation of the magnitude of small events due to an-elastic attenuation (Butcher et al., 2017; Edwards et al., 2015), or whether this is due to differences in the relative frequency of occurrence of small and large earthquakes is an open question. To resolve this question would either require a catalog of **M** values down to a completeness magnitude well below 1 or a careful recalibration of catalog M_L values that avoids the potential danger of overcompensating for the expected underestimation of M_L for small earthquakes. A large data set of synthetic seismograms that simulates the data of a real earthquake catalog in a realistic way would be useful to check the actual calibration procedures and to understand the sensitivity of multi-station M_L values to different parameters.

Acknowledgments

We want to thank Editor Gavin Hayes, David Shelly and another anonymous reviewer for their valuable comments. We also want to thank Peggy Hellweg for introducing us to how catalog magnitudes are calculated in Northern California. This project is partly funded by the Swiss National Science Foundation SNF: Project number 200021_149428. The data used for the earthquake catalog are provided in the Supporting Information file or available from the corresponding author. The figures in this article were made using Generic Mapping Tools (GMT) 5 software written by Wessel and Smith (1998). There are no financial conflicts for any author.

References

Abercrombie, R. E., and J. N. Brune (1994), Evidence for a constant b-value above magnitude 0 in the southern San Andreas, San Jacinto and San Miguel fault zones, and at the Long Valley Caldera, California, Geophys. Res. Lett., 21, 1647– 1650.

Aki, K. and P. G. Richards (2002), “Quantitative Seismology”, 2nd edition, University Science Books, Sausalito.

Aki, K. (1987), Magnitude-frequency relation for small earthquakes: A clue to the origin of fmax of large earthquakes, J. Geophys. Res., 92(B2), 1349–1355.

Atkinson, G. M., and W. Silva (1997). An empirical study of earthquake source spectra for California earthquakes, Bull. Seism. Soc. Am. 87, 97–113.

Bakun,W.H. et al., 2005. Implications for prediction and hazard assessment from the 2004 Parkfield earthquake, Nature, 437, 969–974.

Bakun, W. H. and A. G. Lindh (1985). The Parkfield, California, earthquake prediction experiment. Science, 229, 619–-624

Bakun,W.H. (1984). Seismic moments, local magnitudes, and coda-duration magnitudes for earthquakes in central California, Bull. seism. Soc. Am., 4, 439–458.

Bethmann, F., Deichmann, N. & Mai, P.M. (2011). Scaling relations of local magnitude versus moment magnitude for sequences of similar earthquakes in Switzerland, Bull. Seism. Soc. Am., 101, 515–534.

Brune, J, (1971). Correction: tectonic stress and spectra of seismic shear waves from earthquakes, J. Geophys. Res., 76, 5002.

Brune, J. (1970). Tectonic stress and spectra of seismic shear waves from earthquakes, J. Geophys. Res., 75, 4997 – 5009.

Butcher, A., Luckett, R., Verdon, J.P., Kendall, J.M., Baptie, B. and Wookey, J., 2017. Local magnitude discrepancies for near-event receivers: implications for the UK Traffic-Light Scheme. Bulletin of the Seismological Society of America. https://doi.org/10.1785/0120160225

Deichmann, N. (2017). Theoretical Basis for the Observed Break in ML/**M** Scaling between Small and Large Earthquakes, Bull. Seism. Soc. Am., 107 (2), 250–268, doi: 10.1785/0120160318.

Eaton, J. P. (1997). Determination of amplitude and duration magnitudes and site residuals from short period seismographs in northern Californias, Bull. Seism. Soc. Am., 82, 533-579.

Edwards, B. (2015). The influence of earthquake magnitude on hazard related to induced seismicity, in Perspectives on European Earthquake Engineering and Seismology, A. Ansal (Editor), in Geotechnical, Geological and Earthquake Engineering, Vol. 39, doi: 10.1007/978- 3-319-16964-4_18.

Edwards, B., and J. Douglas (2014).Magnitude scaling of induced earthquakes. Geothermics 52, 132–139, doi: 10.1016/j.geothermics.2013.09.012.

Edwards, B., B. Allmann, D. Fäh and J. Clinton (2010). Automatic Computation of Moment Magnitudes for Small Earthquakes and the Scaling of Local to Moment Magnitude, Geophys. J. Int., 183, 407-420, doi: 10.1111/j.1365-246X.2010.04743.x.

Edwards, B., T. Kraft, C. Cauzzi, P. Kästli, and S. Wiemer (2015). Seismic monitoring and analysis of deep geothermal projects in St. Gallen and Basel, Switzerland, Geophys. J. Int. 201, 1020–1037, doi: 10.1093/gji/ggv059.

Fäh, D., D. Giardini, P. Kästli, N. Deichmann, M. Gisler, G. Schwarz- Zanetti, S. Alvarez-Rubio, S. Sellami, B. Edwards, B. Allmann, et al. (2011). ECOS-09 earthquake catalogue of Switzerland release 2011 report and database, public catalogue, 17/04/2011, Report SED/RISK/ R/001/20110417, Swiss Seismological Service ETH Zurich.

Goertz-Allmann, B.P., Edwards, B., Bethmann, F., Deichmann, N., Clinton, J., Fäh, D. & Giardini, D. (2011). A new empirical magnitude scaling relation for Switzerland, Bull. seism. Soc. Am., 101, 3088–3095.

Gutenberg, B.&Richter, C.F. (1944). Frequency of earthquakes in California, Bull. Seism. Soc. Am., 34, 185–188.

Hanks, T. C., and H. Kanamori (1979). A moment magnitude scale, J. Geophys. Res., 84 (B5), 2348–2350.

Hanks, T.C. & Boore, D.M. (1984). Moment-magnitude relations in theory and practice, J. Geophys. Res., 89, 6229–6235.

Harrington, R.M. & Brodsky, E.E. (2009). Source Duration Scales with Magnitude Differently for Earthquakes on the San Andreas Fault and on Secondary Faults in Parkfield, California, Bull. Seism. Soc. Am., 99 (4), 2323–2334, doi: 10.1785/0120080216.

HRSN (2014), High Resolution Seismic Network. UC Berkeley Seismological Laboratory. Dataset. doi:10.7932/HRSN.

Ide, S., and G. C. Beroza (2001), Does apparent stress vary with earthquake size?, Geophys. Res. Lett., 28(17), 3349–3352, doi:10.1029/2001GL013106.

Kanamori, H., J. Mori, E. Hauksson, T. H. Heaton, L. K. Hutton and L. M. Jones (1993). Determination of earthquake energy release and ML using TERRAscope, Bull. Seism. Soc. Am., 83, 330-346.

Krystek, M., and M. Anton (2007). Aweighted total least-squares algorithm for fitting a straight line, Meas. Sci. Tech. 18, 3438–3442.

Lee, W., H. K. Bennet, and K. L. Meagher (1972). A method of estimating magnitude of local earthquakes from signal duration, U.S. Geol. Surv. Open-File Rept. 28.

Munafò, I., L. Malagnini, and L. Chiaraluce (2016). On the relationship between **M** and ML for small earthquakes, Bull. Seism. Soc. Am., 106 (5), 2402-2408, doi: 10.1785/0120160130.

Raoof, M., Herrmann, R.B., and L. Malagnini (1999). Attenuation and excitation of three component ground motion in southern California, Bull. Seism. Soc. Am., 89, 888–902.

Richter, C.F. (1935). An instrumental earthquake magnitude scale, Bull. Seism. Soc. Am., 25, 1–32.

Ross, Z. E., Y. Ben-Zion, M. C. White, and F. L. Vernon (2016). Analysis of earthquake body wave spectra for potency and magnitude values: Implications for magnitude scaling relations, Geophys. J. Int. 207, 1158–1164, doi: 10.1093/gji/ggw327.

Shi, Y. & B. Bolt (1982), The standard error of the magnitude-frequency *b* value, *Bull. Seismol. Soc. Am.*, *72*, 1677–1687.

Staudenmaier, N., Edwards, B., Tormann, T., Zechar, J. D. & Wiemer, S. (2016). Spatial distribution and energy release of nonvolcanic tremor at Parkfield, California, J. Geophys.Res. Solid Earth, 121, 8833–8854, doi:10.1002/2016JB013283.

Stork, A.L., J.P. Verdon and J.-M. Kendall (2014). The robustness of seismic moment and magnitudes estimated using spectral analysis. Geophysical Prospecting, 62, 862–878 doi: 10.1111/1365-2478.12134.

Takemura, S., Furumura, T. and Saito, T.(2009). Distortion of the apparent *S*-wave radiation pattern in the high-frequency wavefield: Tottori-Ken Seibu, Japan, earthquake of 2000, Geophys. J. Int. 178, 950-961, doi: 10.1111/j.1365-246X.2009.04210.x

Tormann, T., S. Wiemer, E. Hauksson (2010). Changes of reporting rates in the Southern Californian earthquake catalog, introduced by a new definition of ML. *Bulletin of the Seismological Society of America*, Vol. 100

Tormann, T., S..& Hardebeck, J. (2012). Earthquake recurrence models fail when earthquakes fail to reset the stress field, *Geophys. Res. Lett.,* **39**, doi:10.1029/2012GL052913.

Tormann, T., Wiemer, S. & Mignan, A. (2014). Systematic survey of high-resolution b value imaging along Californian faults: inference on asperities, J. Geophys. Res. Solid Earth, 119, 2029–2054, doi:10.1002/2013JB010867.

Uhrhammer, R.A. & Collins, E.R. (1990). Synthesis of Wood-Anderson seismograms from broadband digital records, Bull. Seism. Soc. Am., 80, 702–716.

Wiemer, S., L. Danciu, B. Edwards, M.Marti, D. Fäh, S.Hiemer, J. Wössner, C. Cauzzi, P.Kästli and K.Kremer (2015),Seismic Hazard Model 2015 for Switzerland (SUIhaz2015), Swiss Seismological Service (SED) at ETH Zurich.

Wiemer, S., · D. Giardini, D.Fäh, N. Deichmann and S.Sellami (2009). Probabilistic seismic hazard assessment of Switzerland: best estimates and uncertainties. J Seismol.,13, 449–478. doi:10.1007/s10950-008-9138-7.

Wiemer, S. & Wyss, M. (2002). Mapping spatial variability of the frequency-magnitude distribution of earthquakes, Adv. Geophys., 45, 259–302, doi:10.1016/S0065-2687(02)80007-3.

Figure 1: Distribution of earthquakes along the Parkfield segment with different fault regimes of the SAF : aerial view (with contours representing elevation) : earthquake data and study area (black box). Histogram: number of events in each magnitude bin for the study area. Triangles: HRSN stations (red: Reference station).

Figure 2: Scaling break: a) Observed scaling break in Swiss data (black line: interpolation of Edwards et al., 2015 modified from Goertz-Allmann et al., 2011). b) Observed scaling break in Parkfield data (fit obtained following Edwards et al., 2015).

Figure 3: Frequency magnitude distribution: a) purple: local magnitude; green: duration magnitude; blue: moment magnitude. Red background illustrates transition in scaling at M<2; Inset top: Linear regression between **M** and M_L, illustrating a clear transition in scaling around magnitudes 2-2.5. Inset bottom: Normalized velocity spectra fit (based on Brune's model (Brune, 1970 and 1971): Maximum corner frequency around 30Hz (red line). Blue (light and dark) lines: event spectra. Black line: the frequency response of the attenuation operator (Raoof et al., 1999). Theoretical GR-FMD: b) assuming linear local magnitude (red) FMD. c) assuming linear moment magnitude FMD.

Figure 1.

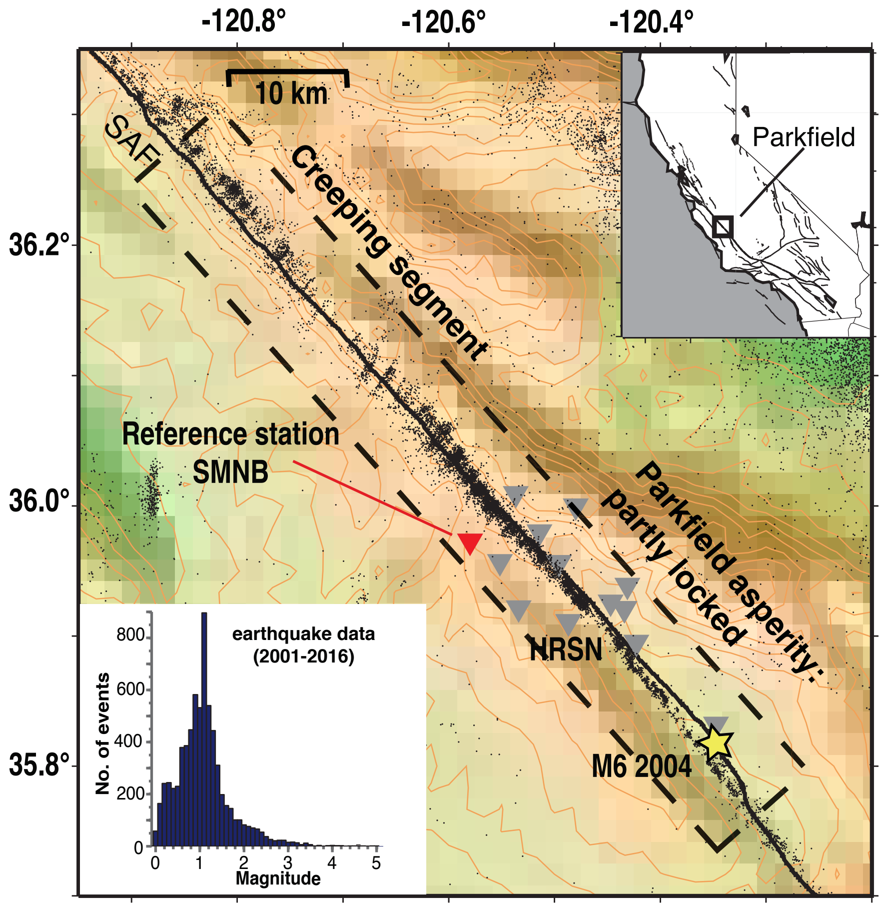

-120.8°
-120.6°
-120.4°
36.2°
36.0°
35.8°
10 km
SAF
Creeping segment
Parkfield
Reference station
SMNB
Parkfield asperity:
partly locked
NRSN
M6 2004
earthquake data
(2001-2016)
No. of events
Magnitude

Figure 2.

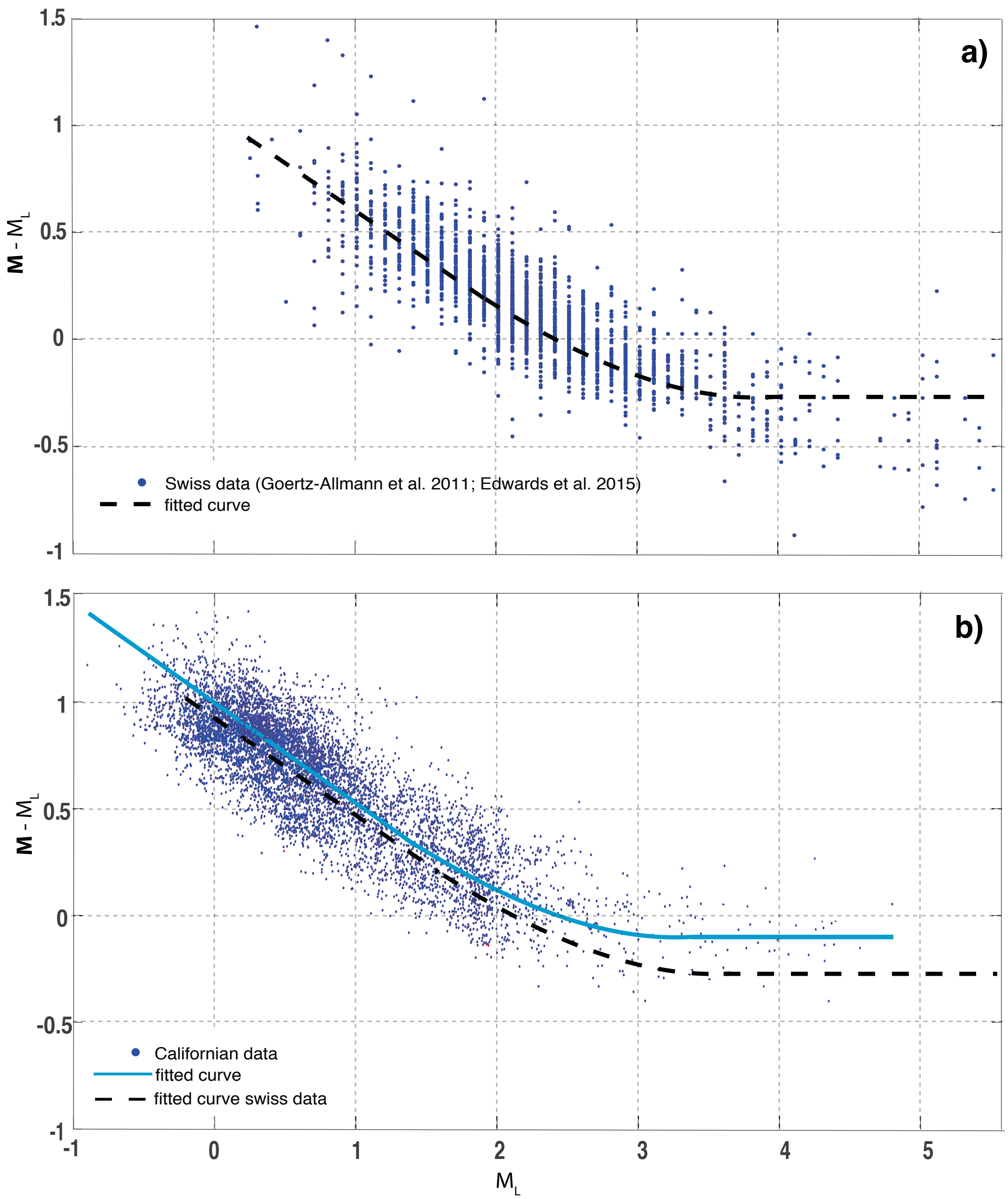

a)
b)
M - M_L
M_L
1.5
1
0.5
0
-0.5
-1
-1
0
1
2
3
4
5
Swiss data (Goertz-Allmann et al. 2011; Edwards et al. 2015)
fitted curve
Californian data
fitted curve
fitted curve swiss data

Figure 3.

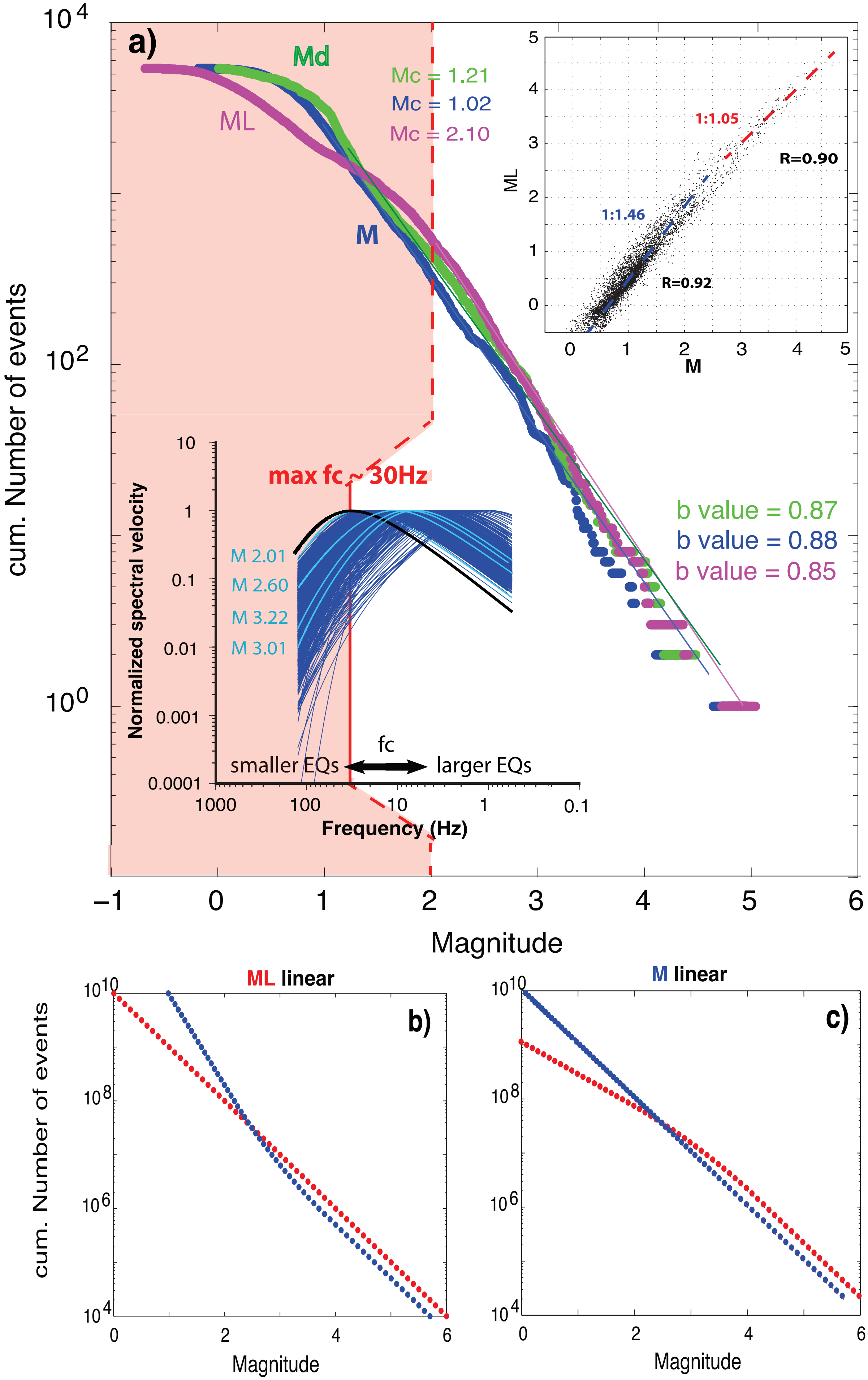

a)
Md
ML
M
Mc = 1.21
Mc = 1.02
Mc = 2.10
1:1.05
1:1.46
R=0.90
R=0.92
ML
M
max fc ~ 30Hz
M 2.01
M 2.60
M 3.22
M 3.01
Normalized spectral velocity
smaller EQs
fc
larger EQs
Frequency (Hz)
b value = 0.87
b value = 0.88
b value = 0.85
cum. Number of events
Magnitude
ML linear
M linear
b)
c)